Total retardance measurements based on the complex Fourier coefficients for the rotating polarizer analyzer system

Geliztle A. Parra-Escamilla [a,b], Joel Cervantes-L [a,*], Jorge L. Flores [a], David I. Serrano-García [a]

[a] *Electro-Photonics Department, University Center of Exact Sciences and Engineering (CUCEI), University of Guadalajara, Av. Revolución No. 1500, CP. 44430 Guadalajara, Jalisco, Mexico*
[b] *Faculty of Engineering, Universidad Panamericana, Álvaro del Portillo 49, Zapopan, Jalisco, 45010, Mexico*

ARTICLE INFO

ABSTRACT

We propose a demodulation algorithm based on the calculus of the complex Fourier coefficients; we used a dual rotating polarizer-analyzer polarimeter to show the feasibility of our proposal. Our demodulation algorithm considers the frequency response obtained by the system, and its possible to calculate the total retardation, fast axis orientation and ellipticity of a sample. Our proposal does not require recovering the full Mueller matrix from getting those parameters. In addition, as the proposal does not use retarders for the measurement, the system presents potential applications for multi-wavelength measurements on phase retardation samples. We show experimental results showing the capabilities of our proposal in characterizing a polarization retardance sample.

1. Introduction

Polarimetry is an experimental technique focused on determining optical properties by analyzing the polarization response of light reflected or transmitted by the sample. Furthermore, the technique is powerful for developing new measurement systems. For example, in the last decade, the atmospheric sensing field has taken advantage of polarization measurements to characterize pollutant particles in the environment [1,2] and predict climate variations [3]. To measure these parameters, remote sensing devices have been developed to detect changes in the properties of reflective objects such as metals and glass, among other materials [4]. In the biomedical field, polarimetry has been successfully used as a marker to identify cancerous tissue in its early stages [5]. In the ophthalmic field, it has been combined with OCT techniques for retinal imaging applications [6].

A polarimeter employing a rotating polarizer and an analyzer without linear retarders, was first proposed by Azzam [7]. Azzam theoretically demonstrated its feasibility and capabilities to recover the coefficients of the partial Mueller matrix and the Jones matrix through common transformations. Subsequently, several authors followed Azzam's approach to recover the ellipticity parameter through the Jones matrix formulae, applied mainly for the analysis of thin films [8–10] in various wavelength regions [11]. Similarly, other authors [12–14] used the Jones matrix approach to recover ellipticity phase information [12,13] with a further improvement by adding a compensator to the system [14] where later other authors proposed a compensation procedure for a polarization-sensitive optical system and tested it with a variable retarder [15], and in Ref. [16], the authors conclude, based on their experimental

---

* Corresponding author.
  E-mail address: joel.cervantes@academicos.udg.mx (J. Cervantes-L).

results, that the dual rotary retarder system is more sensitive to error due to a compensator than to error due to the analyzer or polarizer.

We achieve the full retardance measurement by considering the sample as an elliptical retarder and proposing a demodulation algorithm based on the complex Fourier coefficients. Since our system does not use retarders for the measurement, a compensation procedure that commonly appears when the retarder is not centered on the working wavelength of the system is avoided.

The article is presented as follows: Section 2 shows the theoretical considerations and the demodulation algorithm. In Section 3, we present experimental results varying the retardation parameters of a sample. The results present the complete retardance information from a partial Mueller matrix, Finally, we present our conclusions and final comments.

2. Rotating polarizer-analyzer polarimeter sensitive to elliptical retardation parameters

The proposal setup is composed of a polarization state generator with a light source, a linear polarizer $LP(0°)$ at $0°$ (employed as orientation reference), and a linear polarizer $LP(\theta)$ rotating at rate θ. The polarization state detector consists of a linear polarizer $LP(4\theta)$ rotating at a rate 4θ and a camera to capture the intensity transmitted by the sample. Fig. 1 shows the diagram and the theoretical parameters involved in the system. We consider the sample as an elliptical retarder $ER(\theta_s, \delta_s, \varphi_s)$ with properties of fast axis orientation θ_s, total retardance δ_s, and ellipticity φ_s.

The Mueller matrix of a linear polarizer $LP(\theta)$ for a given angle θ is, Eq. (1) [17–20],

$$LP(\theta) = \frac{1}{2} \begin{bmatrix} 1 & \cos(2\theta) & \sin(2\theta) & 0 \\ \cos(2\theta) & \cos^2(2\theta) & \cos(2\theta)\sin(2\theta) & 0 \\ \sin(2\theta) & \cos(2\theta)\sin(2\theta) & \sin^2(2\theta) & 0 \\ 0 & 0 & 0 & 0 \end{bmatrix}, \tag{1}$$

while for an elliptical retarder $ER(\theta_s, \delta_s, \varphi_s)$ is given by [20]

$$ER(\theta_s, \delta_s, \varphi_s) = \begin{bmatrix} 1 & 0 & 0 & 0 \\ 0 & D^2 - E^2 - F^2 + G^2 & 2(D \bullet E + F \bullet G) & -2(D \bullet F + E \bullet G) \\ 0 & 2(D \bullet E - F \bullet G) & -D^2 + E^2 - F^2 + G^2 & 2(D \bullet G - E \bullet F) \\ 0 & -2(D \bullet F - E \bullet G) & -2(D \bullet G + E \bullet F) & -D^2 - E^2 + F^2 + G^2 \end{bmatrix}, \tag{2}$$

where,

$$D = \cos(2\varphi_s)\cos(2\theta_s)\sin(\delta_s / 2), E = \cos(2\varphi_s)\sin(2\theta_s)\sin(\delta_s / 2), F = \sin(2\varphi_s)\sin(\delta_s / 2), G = \cos(\delta_s / 2) \tag{3}$$

Considering non-polarized light as input, $S_{in} = [S_0, 0, 0, 0]^T$, the output Stokes vector, S_{out}, is

$$S_{out} = LP(4\theta + \varepsilon_2) \bullet ER(\theta_s, \delta_s, \varphi_s) \bullet LP(\theta + \varepsilon_1) \bullet LP(0) \bullet S_{in}, \tag{4}$$

moreover, the detected intensity, I_{out}, is the first element of S_{out} as

$$\begin{aligned} I_{out} = \frac{S_0}{16} &[2 + 2\cos(2\varepsilon_1 + 2\,\theta) + [G^2 - F^2]\cos(-(4\varepsilon_1 - 2\varepsilon_2) + 4\,\theta) + [-2FG]\sin(-(4\varepsilon_1 - 2\varepsilon_2) + 4\,\theta) + 2[G^2 - F^2]\cos(\\ &- (2\varepsilon_1 - 2\varepsilon_2) + 6\,\theta) + [-2FG]\sin(\\ &- (2\varepsilon_1 - 2\varepsilon_2) + 6\,\theta) + [D^2 - E^2 + G^2 - F^2]\cos(2\varepsilon_2 + 8\,\theta) + [2DE - 2FG]\sin(2\varepsilon_2 + 8\,\theta) + 2[D^2 - E^2]\cos((2\varepsilon_1 + 2\varepsilon_2) + 10\,\theta) \\ &+ 2[2DE]\sin((2\varepsilon_1 + 2\varepsilon_2) + 10\,\theta) + [D^2 - E^2]\cos((4\varepsilon_1 + 2\varepsilon_2) + 12\,\theta) + [2DE]\sin((4\varepsilon_1 + 2\varepsilon_2) + 12\,\theta)] \end{aligned} \tag{5}$$

where the parameters (D, E, F, G) are associated with the sample, Eq. (3); θ is related to the rotation rate of the polarizer and $(\varepsilon_1, \varepsilon_2)$ are the alignment error of the initial angles of the polarizer and analyzer, respectively. The detected signal modulated by the rotation rate of the polarizers consists of a series of harmonics distributed at rotation rates of $[2\theta, 4\theta, 6\theta, 8\theta, 10\theta, 12\theta]$, where four sample-related coefficients are obtained as, Eq. (6),
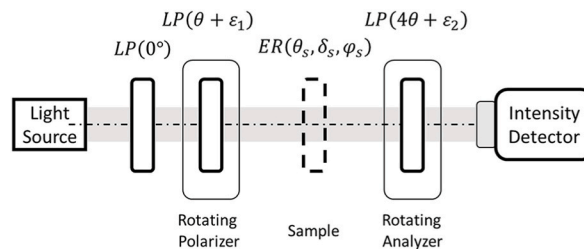

Fig. 1. Rotating polarizer-analyzer polarimeter sensitive to elliptical retardance parameters. *LP*: Linear Polarizer; $(0°, \theta, \theta_s)$: Fast axis orientation of linear polarizers; ER: Elliptical-retarder; δ_s: Total retardance and φ_s: Ellipticity related parameter and where $(\varepsilon_1, \varepsilon_2)$ represents an initial alignment error on the rotating polarizer and analyzer.

$$D^2 - E^2 = \cos(4\theta_s)\cos^2(2\varphi_s)\sin^2\left(\frac{\delta_s}{2}\right), \mathrm{DE} = \frac{1}{2}\sin(4\theta_s)\cos^2(2\varphi_s)\sin^2\left(\frac{\delta_s}{2}\right), \mathrm{G}^2 - \mathrm{F}^2 = \cos^2\left(\frac{\delta_s}{2}\right) - \sin^2\left(\frac{\delta_s}{2}\right)\sin^2(2\varphi_s), \mathrm{FG} = \frac{1}{2}\sin(2\varphi_s)\sin(\delta_s)$$

(6)

In addition, the detected signal can be analyzed through the Fourier transformation. As the output signal is composed of sine-cosine functions with different amplitudes, frequencies, and initial angles, its Fourier transform will be first considered, Eq. (7),

$$F\{\cos(\beta + n\theta)\}(\omega) = \frac{1}{2}\left[e^{-i\beta}\delta(\omega - n) + e^{+i\beta}\delta(\omega + n)\right], F\{\cos(\beta - n\theta)\}(\omega) = \frac{1}{2}\left[e^{+i\beta}\delta(\omega - n) + e^{-i\beta}\delta(\omega + n)\right],$$

$$F\{\sin(\beta + n\theta)\}(\omega) = \frac{i}{2}\left[e^{-i\beta}\delta(\omega - n) - e^{+i\beta}\delta(\omega + n)\right], F\{\sin(\beta - n\theta)\}(\omega) = \frac{i}{2}\left[e^{+i\beta}\delta(\omega - n) - e^{-i\beta}\delta(\omega + n)\right]$$

(7)

where β is the initial angle, n the harmonic coefficient, $\delta(\omega \pm n)$ the shifted Dirac delta function, and ω the frequency domain. As a result, the Fourier transform of the intensity detected, $\widehat{I}_{out}(\omega)$, at Eq. (5) can be obtained as, Eq. (8),

$$\widehat{I}_{out}(\omega) = \sum_{k=-6}^{6} C_{2k}\delta(\omega + 2k)$$

(8)

where C_{2k} represents the complex coefficient that will depend on the sample and the polarizer's and analyzer's initial angle. $\delta(\omega + 2k)$ represents the Dirac delta function displaced at each $2k$ frequency order. Table 1 shows each complex coefficient where it can be noted that the initial angle of the polarizer-analyzer ($\varepsilon_1, \varepsilon_2$) represents a phase variation.

Our approach first removes the constant phase variation obtained by each Fourier coefficient as, Eq. (9),

$$\alpha_{\pm 4} = \frac{2}{C_0}\left[e^{2i(2\varepsilon_1 - \varepsilon_2)}C_4 \pm e^{-2i(2\varepsilon_1 - \varepsilon_2)}C_{-4}\right], \alpha_{\pm 6} = \frac{2}{C_0}\left[e^{2i(\varepsilon_1 - \varepsilon_2)}C_6 \pm e^{-2i(\varepsilon_1 - \varepsilon_2)}C_{-6}\right], \alpha_{\pm 10} = \frac{2}{C_0}\left[e^{-2i(\varepsilon_1 + \varepsilon_2)}C_{10} \pm e^{2i(\varepsilon_1 + \varepsilon_2)}C_{-10}\right]$$

(9)

where $\alpha_{\pm 4,6,10}$ are the complex Fourier order contribution without taking in account the initial angle of the polarizer and analyzer. The sample retardance information is retrieved as

$$\tan(4\theta_s) = i\frac{\alpha_{-10}}{\alpha_{+10}}, \cos(\delta_s) = \frac{1}{2}\left[\alpha_6 - \frac{\alpha_{+10}}{\cos(4\theta_s)}\right], \sin(2\varphi_s) = -i\frac{\alpha_{-4}}{\sqrt{1 - \cos^2(\delta_s)}}$$

(10)

The errors in the angle parameters ($\varepsilon_1, \varepsilon_2$) need to be measured beforehand, for example, by running a measurement without a sample and considering air as a non-polarizing sample. In this manner, the calibration parameters can be obtained as, Eq. (11),

$$\tan(2\varepsilon_1) = \frac{-i(C_{air2} - C_{air-2})}{C_{air2} + C_{air-2}}, \tan(2\varepsilon_2) = \frac{-i(C_{air8} - C_{air-8})}{C_{air8} + C_{air-8}}$$

(11)

with the procedure developed in this section, we can retrieve the sample's information considering a rate rotation of 1:4 on the polarizers and the complex coefficients of the Fourier transform. Comparably, the polar decomposition proposed by Lu-Chipman [17] also employs the total retardance, δ_s, fast axis orientation, θ_s, and the ellipticity angle, φ_s. However, it still employs coefficients from a complete Mueller matrix. Appendix I shows the polar decomposition on the elliptical retarder matrix showing the difference with our demodulation process presented in Eq. (10).

3. Experimental results

We built an experimental setup as presented in Fig. 1. The system uses a He–Ne laser light source operating at 632.8 nm (Thorlabs-HNLS008L). As the first polarizer and orientation reference, we use a Wollaston prism to produce s-polarized light (Thorlabs-WP10). Two dichroic film polarizers were used with an extinction ratio of 492:1 at 405 nm and 803:1 at 520 nm. For the rotating polarizer and

Table 1
Complex coefficients obtained from the Fourier transform of the output signal.

$C_0 = \frac{S_0}{8}$	
$C_2 = \frac{S_0}{16}e^{2i\varepsilon_1}$	$C_{-2} = \frac{S_0}{16}e^{-2i\varepsilon_1}$
$C_4 = -\frac{S_0}{32}e^{-2i(2\varepsilon_1 - \varepsilon_2)}(F - iG)^2$	$C_{-4} = -\frac{S_0}{32}e^{2i(2\varepsilon_1 - \varepsilon_2)}(F + iG)^2$
$C_6 = -\frac{S_0}{16}e^{-2i(\varepsilon_1 - \varepsilon_2)}(F - iG)^2$	$C_{-6} = -\frac{S_0}{16}e^{2i(\varepsilon_1 - \varepsilon_2)}(F + iG)^2$
$C_8 = \frac{S_0}{32}e^{2i\varepsilon_2}((D - iE)^2 - (F - iG)^2)$	$C_{-8} = \frac{S_0}{32}e^{-2i\varepsilon_2}((D + iE)^2 - (F + iG)^2)$
$C_{10} = \frac{S_0}{16}e^{2i(\varepsilon_1 + \varepsilon_2)}(D - iE)^2$	$C_{-10} = \frac{S_0}{16}e^{2i(\varepsilon_1 + \varepsilon_2)}(D + iE)^2$
$C_{12} = \frac{S_0}{32}e^{2i(2\varepsilon_1 + \varepsilon_2)}(D - iE)^2$	$C_{-12} = \frac{S_0}{32}e^{-2i(2\varepsilon_1 + \varepsilon_2)}(D + iE)^2$

analyzer, we employed two motorized rotation devices (Thorlabs – K10CR1). As an intensity detector, we employed a USB power meter (Thorlabs – PM16-121) composed of a photodiode sensor. We combined a liquid crystal cell (LCC) model Thorlabs-LCC1223-A with a quarter-wave plate (WPQ10E-633, Thorlabs) to obtain an elliptical retarder. The system was aligned and built according to the Thorlabs 30 mm optical cage system. In each measurement, we acquired 36 intensities by rotating the first polarizer with 10° increments and the second polarizer with increments of 40°. As our approach is based on the complex Fourier coefficients Fig. 2(b and c) from the detected intensity, Fig. 2 (a) shows the intensity variation obtained with the quarter wave placed at θ_s = -40°. Blue asterisks (*) correspond to the experimental value, while red lines represent the simulation. The performed simulation was based on the Mueller-Stokes matrix multiplication represented by Eq. (4), and also considering the input sample parameters ($\theta_s, \delta_s, \varphi_s$), and initial angles ($\varepsilon_1, \varepsilon_2$) measured with the system. In this case, the root mean square error (RMSE) for the intensity is 0.039.

In the first sets of experiments, we varied the retardance of the LCC, acting as a variable linear retarder where ellipticity and fast axis orientation remain constant. Fig. 3 shows the results obtained where the retardance, δ_s, changes from 0° to 180° while the ellipticity angle was $\varphi_s = -0.21° \pm 2.19°$ and the fast axis orientation was $\theta_s = 2.14° \pm 2.27°$. Blue asterisks (*) correspond to the experimental value, while red lines represent the simulation. To show the feasibility of our measurement, we simulated Eq. (4) considering a variable linear retarder using the mean values of the ellipticity and orientation measured by the dual rotating polarizer-analyzer system Fig. 3(a–c). In this case, the RMSE values between the simulation and the experimental measurement were 1.60°, 2.56°, and 1.43° for the fast axis orientation, total retardance, and the ellipticity value respectively. In addition, we obtain a variation in the fast axis orientation with voltage of 8.05° per volt at 632.8 nm by using a linear regression model with the experimental data. This value is in accordance with reference [21].

In order to show the feasibility of our proposal to use other wavelengths, we performed same measurements at two wavelengths by using a laser light source operating at 520 nm (Thorlabs-PL 201) and other working at 405 (Thorlabs-PL 205). Fig. 4 shows the results obtained in total retardance. The RMS obtained in this case are 2.56° for the light source of 632.8 nm, 5.46° for the light source of 520 nm and 6.60° for the light source of 405 nm. In this case we obtained a shift on the retardance-voltage relation at the linear region. In this case, the variation of the fast axis orientation parameter is 8.05° per volt at 632.8 nm; 0.01° per volt at 520 nm and 2.44° per volt at 405 nm.

In the next experiment, we rotated a quarter wave plate emulating a variation in the fast axis orientation while remaining stable in the parameters of retardance and ellipticity. Fig. 5a–c) shows the results obtained and its representation in the Poincare sphere in Fig. 5 (d) by using the fast axis orientation and the ellipticity. We obtained a value of total retardance of $\delta_s = 93.07° \pm 0.42°$, and ellipticity of $\varphi_s = -051° \pm 0.40°$ at 632.8 nm, and a variation from $-50°$ to 50° at the fast axis orientation part. In the Poincare sphere representation [22], Fig. 5(d), the fast axis orientation represents a variation in the sphere's equator. Asterisks (*) correspond to the experimental value, while the continuous lines represent the simulations. The RMSE values for orientation, retardance, and ellipticity are 0.91°, 0.39°, and 0.38°. Fig. 5(b) shows the results obtained at other two wavelengths for the total retardance. In this case the values of retardance are $\delta_s = 119.5° \pm 0.24°$, and ellipticity $\varphi_s = -0.10° \pm 0.07°$ for 520 nm. In the case of 405 nm, retardance is $\delta_s = 175.31° \pm 4.03°$, and ellipticity $\varphi_s = -1.08° \pm 2.28°$.

Fig. 6 shows the results obtained with an elliptical retarder by combining the LCC and the quarter-wave plate using the light source at 632.8 nm. In this case, we emulate a variable elliptical retarder by fixing the retardance on the LLC at 180° and rotating the quarter wave plate. Simulations were performed according to Eq. (4) considering the mean values of the total retardance and orientation measured by the dual rotating polarizer-analyzer system, Fig. 6(a–c). In the Poincare sphere representation, the ellipticity change corresponds to a variation in the hemisphere; it can also be noted that total retardance varies due to the summation by combining the two linear retarders Fig. 6d). The fast axis orientation is $\theta_s = -0.32° \pm 2.56°$ where the RMSE values obtained for the orientation, retardance, and ellipticity are 2.46°, 10.32°, and 2.34° respectively.
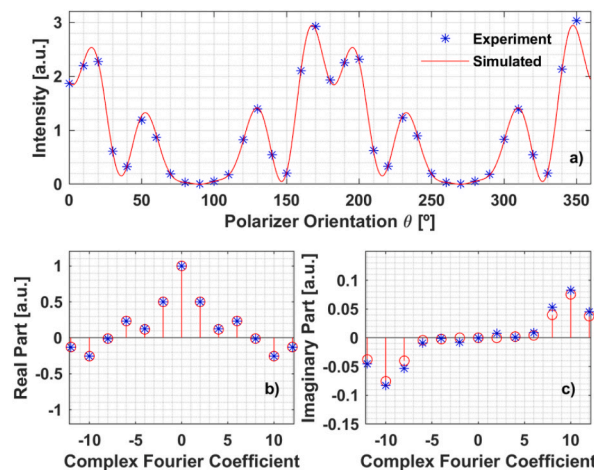

Fig. 2. Intensity variation obtained by placing a quarter wave plate with its fast axis oriented at −40°. (a) Real and (b) imaginary part of the complex Fourier coefficients.
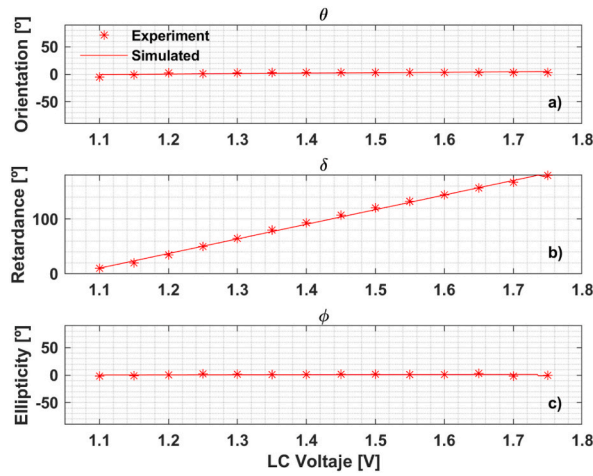
Fig. 3. Experimental results obtained with a variable linear retarder using a liquid crystal cell. (a) Fast axis orientation, (b) total retardance, and (c) ellipticity angle.
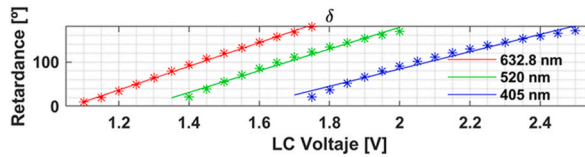

Fig. 4. Total retardance variation obtained with a variable linear retarder using a liquid crystal cell at 632.8 nm (red line), 520 nm (green line) and 405 nm (blue line). (For interpretation of the references to colour in this figure legend, the reader is referred to the Web version of this article.)
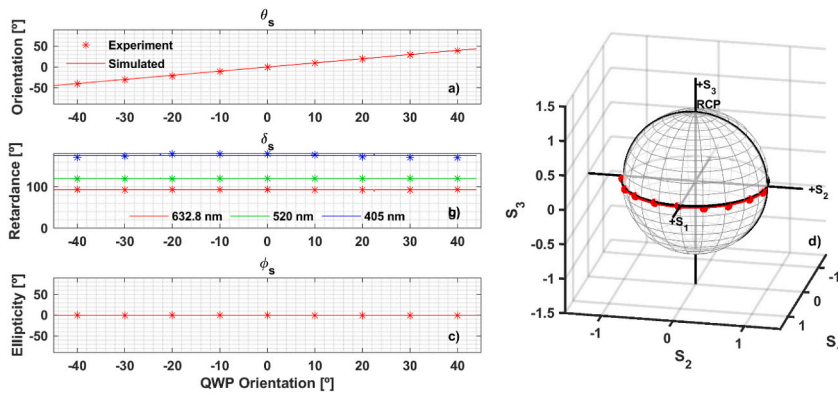

Fig. 5. Experimental results obtained with a rotating quarter wave plate. (a) Fast axis orientation, (b) Total retardance, (c) ellipticity angle, and (d) Poincaré sphere representation.

When comparing our proposal with other systems, such as a complete Mueller matrix polarimeter, the double-rotating retarder system exhibits an intrinsic wavelength dependence due to the retarders. On the contrary, our proposal has the advantage of not using them. Also, compared to the pixelated polarization camera or the approach presented at [21], by employing a rotating analyzer, our model is wider than just measuring only linear retardance information, as we recovered the contribution of ellipticity. One of the limitations of our proposal is that it will be used to measure samples of pure retardance; in the case of diattenuation and depolarization, a more extensive model is required.

4. Conclusion and final remarks

We proposed an algorithm based on the calculation of the Fourier complex coefficients and the system's frequency considering the initial angle of the polarizer and the analyzer as calibration. The algorithm allows us to measure total retardance, orientation, amount
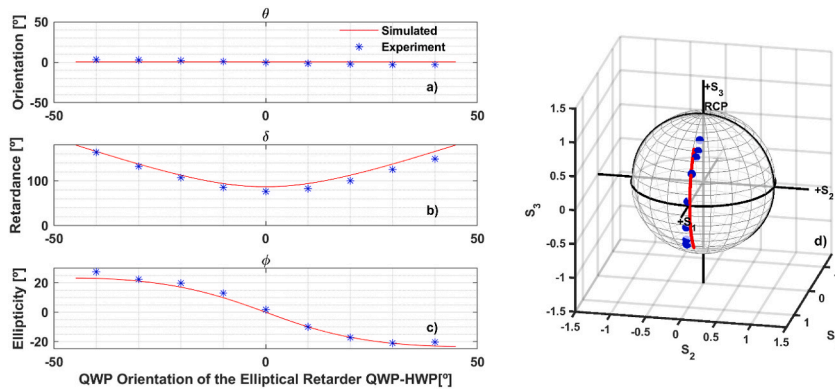
Fig. 6. - Experimental results obtained with an elliptical retarder constructed with a liquid crystal cell (LCC) and a rotating quarter wave plate. (a) Fast axis orientation, (b) total retardance, (c) ellipticity angle, and (d) Poincaré sphere representation.

of retardance, and ellipticity for non-diatenuating and non-depolarizing samples. Since we are recovering the orientation of the fast axis and the ellipticity angle, both angles can represent the sample on the Poincaré sphere. We take advantage of a retardance-sensitive polarimeter based on a rotating polarizer-analyzer setup. The system is focused on recovering the full retardation parameters of a sample by treating it as an elliptic retarder.

Our approach recovers the same retardance information as a complete Mueller matrix polarimeter, even though we have a partial Mueller matrix polarimeter. The implementation presents several advantages compared to other systems that employ retarders with a performance that strongly depends on the wavelength. The concept introduced in this paper could be used for high-bandwidth spectroscopy polarimetry. Another advantage is reducing the implementation cost by using only linear polarizers. In addition, since the system does not use retarders for the measurement, a compensation procedure that commonly appears when the retarder is not centered on the working wavelength of the system is avoided.

Author contribution statement

Geliztle A. Parra-Escamilla, Jorge L. Flores: Conceived and designed the experiments; Analyzed and interpreted the data; Wrote the paper.

Joel Cervantes-L, David I. Serrano-García: Conceived and designed the experiments; Performed the experiments; Analyzed and interpreted the data; Wrote the paper.

Data availability statement

Data will be made available on request.

Declaration of competing interest

The authors declare that they have no known competing financial interests or personal relationships that could have appeared to influence the work reported in this paper.

Acknowledgments

G. A. Parra-Escamilla acknowledges the support provided by the Universidad Panamericana for her postdoctoral project at the same institution.

Appendix I. Polar Decomposition Comparison

Lu and Chipman [17] proposed the polar decomposition by separating the Mueller matrix into three matrices: retardance, diattenuation, and depolarization. The algorithm represents the matrices in a vectorial way that helps their representation in the Poincaré sphere. For the case of a pure retarder, the polar decomposition employs various Mueller matrix coefficients that cannot be directly recovered with the rotating polarimeter of the polarizer-analyzer, see Fig. 7. Using the Mueller matrix polar decomposition of the elliptical retarder in Eq. (2), we obtained the same retardation vector depending on the total retardation, the orientation of the fast axis, and the angle of ellipticity. As can be seen from Eq. (10), our demodulation algorithm recovers similar coefficients, even if we obtain a partial Mueller matrix of the retarder.

$$M = \begin{bmatrix} m_{11} & m_{12} & m_{13} & m_{14} \\ m_{21} & m_{22} & m_{23} & m_{24} \\ m_{31} & m_{32} & m_{33} & m_{34} \\ m_{41} & m_{42} & m_{43} & m_{44} \end{bmatrix}$$

‑ ‑ ‑ Information Retrieved by the Rotating Polarizer-Analyzer Polarimeter

—— Retardance Information by Polar Decomposition

Retardance Vector by Polar Decomposition at Elliptical Retarder Matrix

$$\vec{R} = \frac{R}{\sqrt{4 - (m_{22} + m_{33} + m_{44} - 1)^2}} \begin{bmatrix} m_{34} - m_{43} \\ m_{42} - m_{24} \\ m_{23} - m_{32} \end{bmatrix} = \delta_s \begin{bmatrix} \cos(2\varphi_s)\cos(2\theta_s) \\ \cos(2\varphi_s)\sin(2\theta_s) \\ \sin(2\varphi_s) \end{bmatrix}$$

$$R = |\vec{R}| = \mathrm{Cos}^{-1}\left(\frac{m_{22} + m_{33} + m_{44} - 1}{2}\right) = \delta_s$$

Fig. 7. Polar decomposition on the elliptical retarder matrix and the coefficients employed for its calculations. The retardance vector information can be used to localize the information on the Poincare sphere.

References

[1] T. Liu, S. Yu, X. Zhu, R. Liao, Z. Zhuo, Y. He, H. Ma, In-situ detection method for microplastics in water by polarized light scattering, Front. Mar. Sci. 8 (2021), 739683.

[2] O. Dubovik, Z. Li, M.I. Mishchenko, D. Tanré, Y. Karol, B. Bojkov, B. Cairns, D.J. Diner, W. Reed Espinosa, P. Goloub, X. Gu, O. Hasekamp, J. Hong, W. Hou, K. D. Knobelspiesse, J. Landgraf, L. Li, P. Litvinov, Y. Liu, A. Lopatin, T. Marbach, H. Maring, V. Martins, Y. Meijer, G. Milinevsky, S. Mukai, F. Parol, Y. Qiao, L. Remer, J. Rietjens, I. Sano, P. Stammes, S. Stamnes, X. Sun, P. Tabary, L.D. Travis, F. Waquet, F. Xu, C. Yan, D. Yin, Polarimetric remote sensing of atmospheric aerosols: instruments, methodologies, results, and perspectives, J. Quant. Spectrosc. Radiat. Transf. 224 (2019), 747–511.

[3] D. Li, N. Zeng, D. Zhan, Y. Chen, M. Zeng, H. Ma, Differentiation of soot particulates in air using polarized light scattering method, Appl. Opt. 56 (14) (2017) 4123–4129.

[4] K. Ramesh, S. Sasikumar, Digital photoelasticity: recent developments and diverse application, Opt. Laser. Eng. 135 (2020), 106186.

[5] T. Novikova, A. Pierangelo, A.D. Martino, A. Benali, P. Validire, Polarimetric imaging for cancer diagnosis and staging, Opt. Photon. News 23 (10) (2012) 26–33.

[6] B. Cense, D.T. Miller, B.J. King, T. Theelen, A.E. Elsner, Measuring polarization changes in the human outer retina with polarization-sensitive optical coherence tomography, J. Biophot. 11 (5) (2018).

[7] R.M.A. Azzam, Photopolarimetric measurement of the Mueller matrix by Fourier analysis of a single detected signal, Opt. Lett. 2 (6) (1978) 148–150.

[8] R.M.A. Azzam, A simple Fourier photopolarimeter with rotating polarizer and analyzer for measuring Jones and Mueller matrices, Opt. Commun. 25 (2) (1978) 137–140.

[9] M. Gilliot, A.E. Naciri, Theory of dual-rotating polarizer and analyzer ellipsometer, Thin Solid Films 540 (2013) 46–52.

[10] M. Taher, El-Agez, Sofyan Taya, Development and construction of rotating polarizer analyzer ellipsometer, Opt. Laser. Eng. 49 (4) (2011) 507–513.

[11] Sofyan Taya, Taher M. El-Agez, Effect of noise on the optical parameters extracted from different ellipsometic configurations, Phys. Scr. 85 (4) (2012), 45706.

[12] G.Q. Xia, R.J. Zhang, Y.L. Chen, H.B. Zhao, S.Y. Wang, S.M. Zhou, Y.X. Zheng, Y.M. Yang, L.Y. Chen, New design of the variable angle infrared spectroscopic ellipsometer using double Fourier transforms, Rev. Sci. Instrum. 71 (7) (2000), 2677.

[13] S.Y. Berezhna, I.V. Berezhnyy, M. Takashi, Dynamic photometric imaging polarizer-sample-analyzer polarimeter: instrument for mapping birefringence and optical rotation, J. Opt. Soc. Am. A 18 (3) (2001) 666–672.

[14] S.Y. Berezhna, I.V. Berezhnyy, M. Takashi, Integrated photoelasticity through imaging Fourier polarimetry of an elliptic retarder, Appl. Opt. 40 (5) (2001) 644–651.

[15] S.Y. Berezhna, I.V. Berezhnyy, M. Takashi, High-resolution birefringence imaging in three-dimensional stressed models by Fourier polarimetry, Appl. Opt. 40 (28) (2001) 4940–4946.

[16] G. Piller, L. Broch, L. Johann, Experimental study of the systematic errors for a Mueller matrix double rotating compensator ellipsometer, Phys. Status Solidi C 5 (2008) 1027–1030.

[17] S.Y. Lu, R.A. Chipman, Interpretation of Mueller matrices based on polar decomposition, J. Opt. Soc. Am. A 13 (5) (1996) 1106–1113.

[18] D. Goldstein, Polarized Light, second ed., Marcel Dekker Inc., New York, 2003.

[19] Michael Bass, et al., Handbook of Optics: Vol. I–Geometrical and Physical Optics, Polarized Light, Components and Instruments, third ed., McGraw-Hill Professional, New York, 2009.

[20] David S. Kliger, James W. Lewis, Polarized Light in Optics and Spectroscopy, second ed., Elsevier, New York, 2012.

[21] P. Terrier, J.M. Charbois, V. Devlaminck, Fast-axis orientation dependence on driving voltage for a Stokes polarimeter based on concrete liquid-crystal variable retarders, Appl. Opt. 49 (2010) 4278–4283.

[22] J. Roth, Poincare sphere plot of polarimetry Stokes vectors, MATLAB Central File Exchange, https://www.mathworks.com/matlabcentral/fileexchange/10979-poincare-sphere-plot-of-polarimetry-stokes-vectors, 2023 (accessed Dec 17, 2022).